ISSN 0038-0946, Solar System Research, 2017, Vol. 51, No. 5, pp. 362–372. © Pleiades Publishing, Inc., 2017.
Original Russian Text © V.I. Shematovich, D.V. Bisikalo, J.-C. Gérard, B. Hubert, 2017, published in Astronomicheskii Vestnik, 2017, Vol. 51, No. 5, pp. 392–403.

Changes in the Martian Atmosphere Induced by Auroral Electron Precipitation

V. I. Shematovich[a], *, D. V. Bisikalo[a], J.-C. Gérard[b], and B. Hubert[b]

[a] *Institute of Astronomy, Russian Academy of Sciences, Moscow, Russia*
[b] *Department of Astrophysics, Geophysics and Oceanography, University of Liege, Belgium*
**e-mail: shematov@inasan.rssi.ru*

Received February 27, 2017

Abstract—Typical auroral events in the Martian atmosphere, such as discrete and diffuse auroral emissions detected by UV spectrometers onboard ESA *Mars Express* and NASA *MAVEN*, are investigated. Auroral electron kinetic energy distribution functions and energy spectra of the upward and downward electron fluxes are obtained by electron transport calculations using the kinetic Monte Carlo model. These characteristics of auroral electron fluxes make it possible to calculate both the precipitation-induced changes in the atmosphere and the observed manifestations of auroral events on Mars. In particular, intensities of discrete and diffuse auroral emissions in the UV and visible wavelength ranges (Soret et al., 2016; Bisikalo et al., 2017; Gérard et al., 2017). For these conditions of auroral events, the analysis is carried out, and the contribution of the fluxes of precipitating electrons to the heating and ionization of the Martian atmosphere is estimated. Numerical calculations show that in the case of discrete auroral events the effect of the residual crustal magnetic field leads to a significant increase in the upward fluxes of electrons, which causes a decrease in the rates of heating and ionization of the atmospheric gas in comparison with the calculations without taking into account the residual magnetic field. It is shown that all the above-mentioned impact factors of auroral electron precipitation processes should be taken into account both in the photochemical models of the Martian atmosphere and in the interpretation of observations of the chemical composition and its variations using the ACS instrument onboard *ExoMars*.

Keywords: Solar System, Mars, solar wind, high-energy electron precipitation, auroral phenomena, kinetic Monte Carlo method

DOI: 10.1134/S0038094617050094

INTRODUCTION

Observations of aurorae are widely used to analyze the composition, structure, and chemistry of the atmosphere under study as well as fluxes of energy and particles affecting the atmosphere. The aurorae were discovered on all planets with relatively dense atmospheres and on some satellites. In the case of planets with intrinsic magnetic fields, planetary aurorae are discrete events, and if there is no magnetic field, they are diffuse events. The planet Mars is an interesting intermediate case because some regions of the planet have retained residual magnetism, which was trapped in the planetary crust about four billion years ago, while in other regions of the planet there is almost no intrinsic magnetic field. That is why both discrete and diffuse aurorae were discovered on Mars (Schneider et al., 2015).

For the first time, discrete ultraviolet (UV) aurorae were discovered in limb observations using the UV spectrograph of the SPICAM instrument on board *Mars Express* (*MEX*) (Bertaux et al., 2005). Further observations were made in the nadir direction in regions of the planet with a residual magnetic field (Leblanc et al., 2008). In (Gérard et al., 2015), the results of the analysis of the complete MEX/SPICAM observational database were presented to identify the signs of UV emissions in CO Cameron and CO_2^+ doublet bands in aurorae and to analyze simultaneous measurements of electron fluxes precipitating into the atmosphere using the MEX/ASPERA-3/ELS instrument onboard *Mars Express*. The spectral characteristics of auroral emissions were found near the boundary region between the open and closed field lines of the residual magnetic field. The average energy of electrons measured during maximum precipitation fluxes varied from 150 to 280 eV.

As noted in (Schneider et al., 2015), discrete aurorae were detected in the regions of strong crustal magnetic fields and their excitation is explained by the electron precipitation with kinetic energies up to 1 keV that were probably accelerated by parallel electric fields like discrete aurorae on the Earth. In (Brain et al., 2006), measurements that were performed on board *MGS* (*Mars Global Surveyor*) were presented.

They showed that downward electron fluxes are generally almost isotropic for energies ranging from 100 eV to 1 keV.

A new type of aurorae, the so-called diffuse aurorae, whose characteristics differ significantly from discrete aurorae, was discovered in observations using the IUVS spectrograph (Imaging UV Spectrograph) on board NASA *MAVEN* (*Mars Atmosphere Volatile EvolutioN*) (Schneider et al., 2015). Diffuse aurorae cover a significant part (~35° in latitude) of the northern hemisphere of Mars. It is quite probable that aurorae could be even more extended in latitude, but the determination of the geographic dimensions of emissions was limited by the capabilities of the IUVS instrument. The profiles obtained in the limb observations show that diffuse aurorae propagate down to an altitude of ~60 km. Thus, the peak brightness of the event on December 2014 was observed at an altitude of about 70 km (Schneider et al., 2015). Its value reached about 400 rayleigh for the UV doublet CO_2^+. Emissions were also observed in CO Cameron bands, emission of atomic oxygen OI at 297.2 nm, a short-wave emission segment between near UV and optical wavelengths in CO_2^+ Fox–Duffendack–Barker (FDB) bands and other emissions in the far UV range. These aurorae lasted for several days after a period of active solar flares. Simultaneous measurements of energetic electrons using Solar Wind Electron Analyzer (SWEA) and Solar Energetic Particle (SEP) instruments on *MAVEN* showed that the observed UV emissions are caused by electrons with energies up to 200 keV.

The first evidence for the precipitation of energetic electrons was presented in a paper (Brain et al., 2006), in which a peak was noted in electron distributions measured at an altitude of about 400 km using the MGS/ER (Electron Reflectometer) on board NASA *MGS* (*Mars Global Surveyor*). These observations revealed hundreds of events that were characterized by the precipitation of energetic electrons with a maximum energy in the range from ~200 eV to 4 keV. In these events, characteristics of energetic electrons are similar to those of electron populations in aurorae observed in the cusp area of the residual crustal magnetic field. In (Brain et al., 2006), it was suggested that these aurorae occur in magnetic field tubes that connect the solar wind plasma after the detached shock front passage with residual crustal magnetic fields. It was also noted that the electron fluxes precipitating into the atmosphere within the energy range from 100 eV and up to 1 keV are usually almost isotropic. The brightest auroral events are predominantly observed during periods of perturbed solar wind, for example, during the passage of coronal mass ejections.

Measurements carried out using the ASPERA-3 plasma instruments (Analyzer of Space Plasma and Energetic Atoms) on board *Mars Express* (Barabash et al., 2006) also showed that regions of the open magnetic field are often near the regions of the planetary crust with a strong and moderate magnitudes of the residual field on the night side of Mars (Lundin et al., 2006a; 2006b). The electrons associated with these regions are generally characterized by flux values several orders of magnitude higher than elsewhere on the night side, with an inverted V-shaped energy distribution and a peak at energies of several hundred eV. In (Lundin et al., 2006b), it was shown that these electron distributions show signs of a downward acceleration in the upward electric field. It is well known that the precipitation of energetic particles is a very important process everywhere in astrophysical objects, from interacting binary stars to exoplanets (Bisikalo and Shematovich, 2015). In order to investigate the auroral electron precipitation into the rarefied atmospheric layers, it is necessary to solve Boltzmann kinetic equations taking into account electron transport and production of primary and secondary electrons as well as elastic and inelastic scattering. In (Lillis and Brain, 2013), a thorough analysis of the downward electron fluxes with superthermal energies measured by *MGS* at an altitude of about 400 km on the night side of Mars was carried out for the discrete aurora case. In (Lillis et al., 2011,) and (Lillis and Brain, 2013), it was noted that the size and topology of the residual magnetic field of the Martian crust affect the nature of precipitation. These field strength variations and the geographic structure of the shielding effect of the residual magnetic field of the Mars' crust illustrate a complex relationship in the interaction between this field and the solar wind. Energy distributions of high-energy electrons on the nightside of Mars in regions with a stronger residual magnetic field were further investigated in (Shane et al., 2016). They showed that most of the precipitating electrons have energies within the range 15–30 eV, and because of the reflection of the incident flux due to the magnetic field or collisions with atmospheric particles only a small fraction (less than 16%) of electrons loses its energy in the Martian atmosphere.

In (Bisikalo et al., 2017), a Monte Carlo model of electron transport was used to investigate the contribution of the residual magnetic field to the upward and downward fluxes of electrons and to the brightness of auroral emissions. Calculations using the fluxes of precipitating electrons measured by the ASPERA-3 instrument on board *MEX* showed that the magnetic mirroring increases the energy flux carried by upward moving electrons from a relative value of about 20% for the case without the residual crustal magnetic field and up to 33–78% depending on the topology of the residual magnetic field. Conservation of the particle flux in the magnetic flux tube implies that the presence of the magnetic field does not noticeably change emission intensity profiles for the initially isotropic pitch angle distribution. However, it was found that the residual magnetic field leads to an increase in the mirrored electron flux and, consequently, to a decrease in the total auroral brightness for a given

energy flux of precipitating electrons. The fact that the emission peak of the diffuse aurora is located at an altitude of about 70 km is a clear indication of the presence of high-energy electrons in the precipitating flux. For discrete auroral emissions observed by the SPICAM instrument on board *MEX*, the brightness peak is at an altitude of ~140 km (Soret et al., 2016), where the atmospheric pressure is lower by more than two orders of magnitude. Thus, the diffuse aurora is excited by charged particles that penetrate the atmosphere much deeper than the electrons that usually cause a discrete aurora.

The model of the diffuse auroral emission profile in the limb was first presented in (Schneider et al., 2015). They used the analytical approximation for the energy spectrum of electrons based on measurements by the SEP and SWEA instruments on *MAVEN* at an altitude of 400 km during the event in December 2014. According to this approximation, the total electron distribution approximately follows the power law with an exponent of –2.2 in the energy range from ~10 to 200 keV. In the model (Schneider et al., 2015), electron energy is degraded by collisions in a neutral atmosphere, which included three components (CO_2, N_2, and O) from the Mars climate database (Millour et al., 2014). The solution of the transport equation made it possible to calculate the electron flux, which was later used to calculate the volume and column emission rates. In particular, the height profile of the UV emission CO_2^+ was calculated, which corresponds well to observations. Although it was necessary to scale the calculated emission intensity in order to approximate the brightness at the peak altitude measured by the IUVS spectrograph on *MAVEN*. In (Gérard et al., 2017), the variation of the brightness peak altitude of diffuse aurorae was investigated as a function of the initial electron energy. In particular, it was investigated the relative importance of processes involving the molecules and atoms of CO_2, CO, and O as targets causing the excitation in the CO Cameron band and the fourth positive band of the ion CO_2^+, as well as emissions of oxygen at wavelengths of 130.4 and 297.2 nm and carbon multiplets at 156.1 and 165.7 nm.

This paper continues the investigation of the process of electron penetration into the Martian atmosphere, which causes both discrete and diffuse auroral glows, within the models from (Bisikalo et al., 2017) and (Gérard et al., 2017) and provides estimates of the physical effects induced by electron precipitation. The main focus is on the additional heating of the atmosphere due to electron precipitation, changes in the ionization degree, analysis of possible changes in the chemical composition of the atmosphere, etc. Finally, the possibilities of observing changes in the chemical composition of the Martian atmosphere caused by electron precipitation using the ACS (Atmospheric Chemistry Suite) instrument onboard *ExoMars* are discussed.

MODEL

Brief Description of the Monte Carlo Electron Transport Model

In this study, a numerical model of electron transport in the planetary atmosphere was used (Shematovich et al., 2008) which is based on the kinetic Monte Carlo method. Previously, this model was adapted to the atmospheres of Venus (Gérard et al., 2008) and Mars (Shematovich et al., 2008; Soret et al., 2016; Bisikalo et al., 2017; Gérard et al., 2017) to investigate the intensities of auroral glows in the limb and zenith directions in the CO_2-dominant atmosphere excited by high-energy electron precipitation.

Energetic electrons from the induced magnetosphere of Mars can penetrate (precipitate) and interact with a neutral atmosphere, where they lose their kinetic energy in elastic, inelastic, and ionization collisions with atmospheric gas. Energy losses of precipitating electrons are calculated using the Boltzmann kinetic equation (Shematovich et al., 2008), which includes the processes of electron transport, production of primary and secondary electrons, and collision integrals for elastic and inelastic scattering. The kinetic Monte Carlo method is an effective approach for solving the Boltzmann kinetic equation for atmospheric systems in the stochastic approximation, when the number of electron collisions in each cell and the electron transport are considered separately at each time step, in contrast, for example, to the frequently used test particle Monte Carlo method (Lillis et al., 2009, 2011). A more detailed description of the kinetic Monte Carlo model is given in (Shematovich et al., 2008, and Bisikalo and Shematovich, 2015).

The density and temperature profiles of the model neutral atmosphere were taken from the calculations with the global circulation model for Mars, Mars Global Ionosphere-Thermosphere Model (MITM) (Bougher et al., 2015). The M-GITM model takes into account most of the fundamental physical parameters, ion-neutral chemistry, and basic radiation processes on Mars from the surface to the exosphere (0–300 km). In order to investigate the discrete aurora, the atmospheric parameters were calculated for solar longitude 0°, latitude 50° of the southern hemisphere, and longitude 180° (which corresponds to a region with a significant residual magnetic field on Mars), the solar activity index F10.7 was assumed to be 30 for Mars (mean value for the time of auroral events detections), and for the local midnight. In order to investigate the diffuse aurorae, atmospheric gas characteristics were calculated in the M-GITM model with parameters corresponding to detection conditions of a diffuse glow on December 24, 2014, by the IUVS spectrograph on *MAVEN*, namely, local time 24:00, northern latitude 62.5°, longitude 270°, solar activity index 160 (near the Earth). In order to reduce the influence of boundary effects, the lower boundary of the investigated

region of the atmosphere was taken at an altitude of 30 km, and the upper one was set at an altitude of 300 km.

The processes that determine the relative role of all possible collisions and the electron energy loss in these collisions were listed in (Shematovich et al., 2008). Note only that the cross sections for the dissociative excitation and electron-impact ionization of the ground and electronic excited states of the CO_2 molecule and their analytic expressions were taken from (Shirai et al., 2001).

The Monte Carlo electron transport model is based on several assumptions. Firstly, it is assumed that the surrounding atmospheric gas is characterized by the local Maxwell velocity distribution function. Secondly, it is assumed that the electrons precipitate along the lines of the residual crustal magnetic field on Mars, which are considered to be perpendicular to the surface of the planet. Thirdly, the initial distribution of pitch angles of the precipitating electrons is assumed to be isotropic in the sense defined in (Decker et al., 1996), i.e., it is homogeneous in the distribution of the function $\cos^2(\theta)$, where θ is the electron pitch angle.

Used Residual Magnetic Field Model

The vertical structure of the magnetic field is similar to the model used in (Lillis et al., 2009) to analyze the effect of the crustal field on the electron pitch angle distribution (PAD). Since the electron gyroradius takes values of less than a few kilometers at energies below 1 keV for the values of the Martian residual field strength, it is possible to consider electrons conjugated to one line of the residual magnetic field. We also confine ourselves to the approximation of the vertical line of the magnetic field perpendicular to the layers of the model atmosphere but taking into account the concentration of the field lines with decreasing altitude. Then, depending on the distance above the source in the planetary crust the residual magnetic field strength is given by the following approximate formula:

$$B(h) = B_{\text{amb}} + B_{\text{crust, 100 km}} \times [(100\ \text{km}/(h + a)]^k,$$

where h is the height, a is the field source depth in the crust (it is assumed that the source is located 15 km below the surface), $B_{\text{crust, 100 km}}$ is this value of the residual field at a height of 100 km, and k is the parameter that can vary between 2 and 3. In the calculations presented in this paper, the standard values of the parameters $k = 2.5$, $B_{\text{crust, 100 km}} = 23$ nT were used (Lillis et al., 2009). The constant ambient magnetic field B_{amb} was assumed to be 12 nT, which is a typical value of the magnetic field in the tail of the induced Mars magnetosphere. It was also assumed that the electrons were accelerated above the upper boundary of the investigated region, so that the accelerating electrostatic potential in the investigated layers of the atmosphere was assumed to be zero.

CALCULATION RESULTS

Discrete Auroral Events

In order to investigate the effect of precipitating electrons on the state of the upper Martian atmosphere, several calculations were carried out using the kinetic Monte Carlo model. To associate the calculations to the actual observations, the measured values of the electron fluxes obtained in observations carried out by the ASPERA-3 instrument onboard *MEX* were used as the boundary condition at the upper boundary of the numerical model, where the electron flux precipitating into the atmosphere is defined. For simulation, we used the electron energy distribution function detected on May 10, 2010, at 07:44 UT at an altitude of 590 km (Gérard et al., 2015). The energy distribution of the downward electron flux from the upper boundary of the model is shown in Fig. 1. The magnitude of the energy flux decreases strongly for energies above 200 eV and reaches very low values at 300 eV. The peak of the energy flux is observed near the energy of 90 eV, the average electron energy is ~140 eV (Gérard et al., 2015), and the energy flux is 1.4 erg $\text{cm}^{-2}\ \text{s}^{-1}$.

The main result of calculations using a numerical model based on the kinetic Monte Carlo method is the distribution functions by kinetic energy (EDF) of auroral electrons as well as the energy spectra of the upward and downward electron fluxes. The calculations were carried out both taking into account the residual crustal magnetic field of Mars, when $B_{\text{crust, 100 km}} = 23$ nT, and without taking it into account, when $B_{\text{crust, 100 km}} = 0$ nT. As noted above, in calculations it was assumed that the crustal magnetic field has typical parameters: $a = 15$ km, $k = 2.5$, and $B_{\text{amb}} = 12$ nT, the flux of precipitating electrons at the upper boundary was assumed to be equal to that measured using the ASPERA-3 instrument on board *MEX* on May 10, 2010, at 07:43. Figure 2a shows the electron kinetic energy distribution functions, and Figs. 2b and 2c show calculations of the energy spectra of the downward and upward fluxes of auroral electrons, respectively. The energy flux of electrons precipitating into the Martian atmosphere at an altitude of 241 km almost coincides with the electron flux measured by the ASPERA-3 instrument on board *MEX* (Fig. 1), which indicates the low impact of the upper (above 241 km) atmosphere on the precipitating flux. As the particle flux penetrates deep into the atmosphere, its value decreases. Simulation results showed that under the adopted parameters the upward energy flux reaches a fraction of 33% of the downward one. It is important to note that at low energies in the formation of the thermal core of the upward flux an important role is played by collisional redistribution of pitch angles in the generation of an upward flux of electrons. At high energies, the upward flux is formed mainly due to the magnetic mirroring. In the case of $B_{\text{crust, 100 km}} = 0$ nT there is no contribution from the magnetic mirroring, which leads to a significant decrease in the

numerical upward flux for energies above ~10 eV. This, in turn, leads to a significant reduction, up to 20%, of the fraction of the upward (reflected by the atmosphere) energy flux. Thus, from the analysis of the calculations presented in Figs. 2b and 2c it can be concluded that the effect of the residual crustal magnetic field of Mars leads to a noticeable, energy-dependent increase in the fraction of the upward electron energy flux from 20 to 33% (Bisikalo et al., 2017).

Kinetic energy distribution functions and energy spectra of the upward and downward electron fluxes of auroral electrons obtained in calculations make it possible to calculate the observed manifestations of auroral events on Mars, in particular, the intensities of discrete and diffuse aurorae in the UV and visible wavelength bands (Soret et al. 2016; Bisikalo et al., 2017; Gérard et al., 2017).

Auroral electron distribution functions also make it possible to estimate the contribution of electron precipitation to the aeronomy of the upper Martian atmosphere. Knowledge of these functions makes it possible to assess the efficiency of heating the atmospheric gas by precipitating auroral electrons with taking into account the residual crustal magnetic field (Fig. 3a) and without taking it into account (Fig. 3b). Accordingly, bottom panels of Figs. 3a and 3b show the altitude profile of the atmospheric gas heating efficiency as the ratio of the deposition and heating rates by precipitating electrons presented on the top panels. It can be seen that the heating efficiency varies greatly with altitude in the upper atmosphere and, if there is no residual magnetic field, a larger electron flux penetrates deeper into the atmosphere, which leads to a higher atmospheric gas heating efficiency (see, Figs. 3a and 3b, bottom panels). Presented calculated values should be used in the investigation of the thermal state of the upper Martian atmosphere for discrete auroral events.

Figure 4 shows the results of calculating the ionization rates of the main components of the upper Martian atmosphere due to auroral electron precipitation with taking into account the residual crustal magnetic field (Fig. 4a) and without taking it into account (Fig. 4b). It can be seen that in the case of calculation without taking into account the residual magnetic field ionization rate peaks become are placed at lower altitudes while their values increase by 10–20%. The calculated ionization rates of the atmospheric gas due to auroral electron precipitation should be used in aeronomical models of Martian photochemistry and also in considering the evolution and subsequent loss of the Martian atmosphere, especially when investigating the role of extreme solar events, i.e., solar flares and coronal mass ejections, as evidenced by recent observations on NASA *MAVEN* (Jakosky et al., 2015; Schneider et al., 2015).

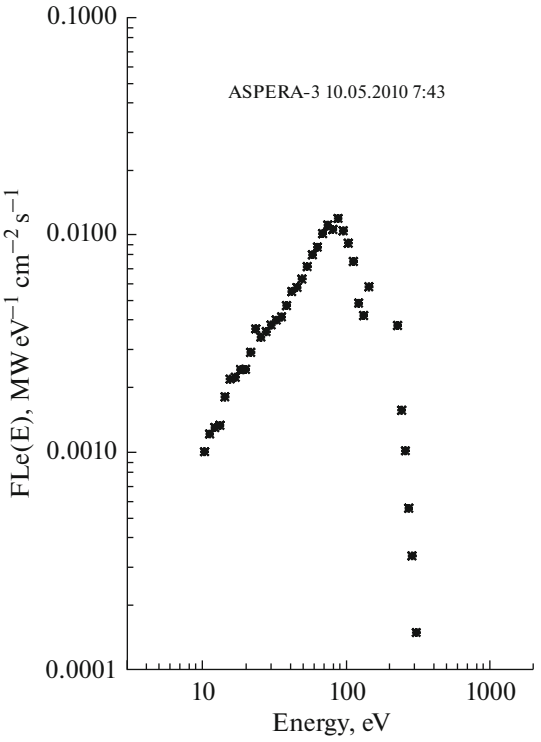

Fig. 1. Energy spectrum of the energy flux FLe of precipitating electrons measured at an altitude of 590 km on May 10, 2010, at 7:43 UT using the ASPERA-3 instrument on board *Mars Express*.

Diffuse Auroral Events

As noted above, diffuse auroral events are caused by precipitation of electrons the energy spectrum of which follows a power law with a exponent of –2.2 in the energy range from ~10 to 200 keV in accordance with measurements of SEP and SWEA instruments on *MAVEN* at an altitude of 400 km during the event in December 2014 (Jakosky et al., 2015; Schneider et al., 2015). Electron precipitation is effectively simulated using the kinetic Monte Carlo model of diffuse auroral events with a complex energy spectrum by calculating the penetration from the upper boundary of the model of monoenergetic electron fluxes with characteristic energies E_0 in the range from 10 to 200 keV. In our calculations, the initial pitch angle distribution of electrons precipitating at the upper boundary of the model was assumed to be isotropic. In each case, the energy flux of precipitating electrons was set equal to 1 mW cm^{-2} s^{-1}. In order to estimate the observed brightnesses of diffuse aurorae, it is necessary to scale these calculations with monoenergetic electron fluxes with energies in the range from 10 to 200 keV in accordance with electron energy fluxes for the investigated diffuse auroral event measured by SEP and SWEA instruments on *MAVEN* (Bisikalo et al., 2017; Gérard et al., 2017).

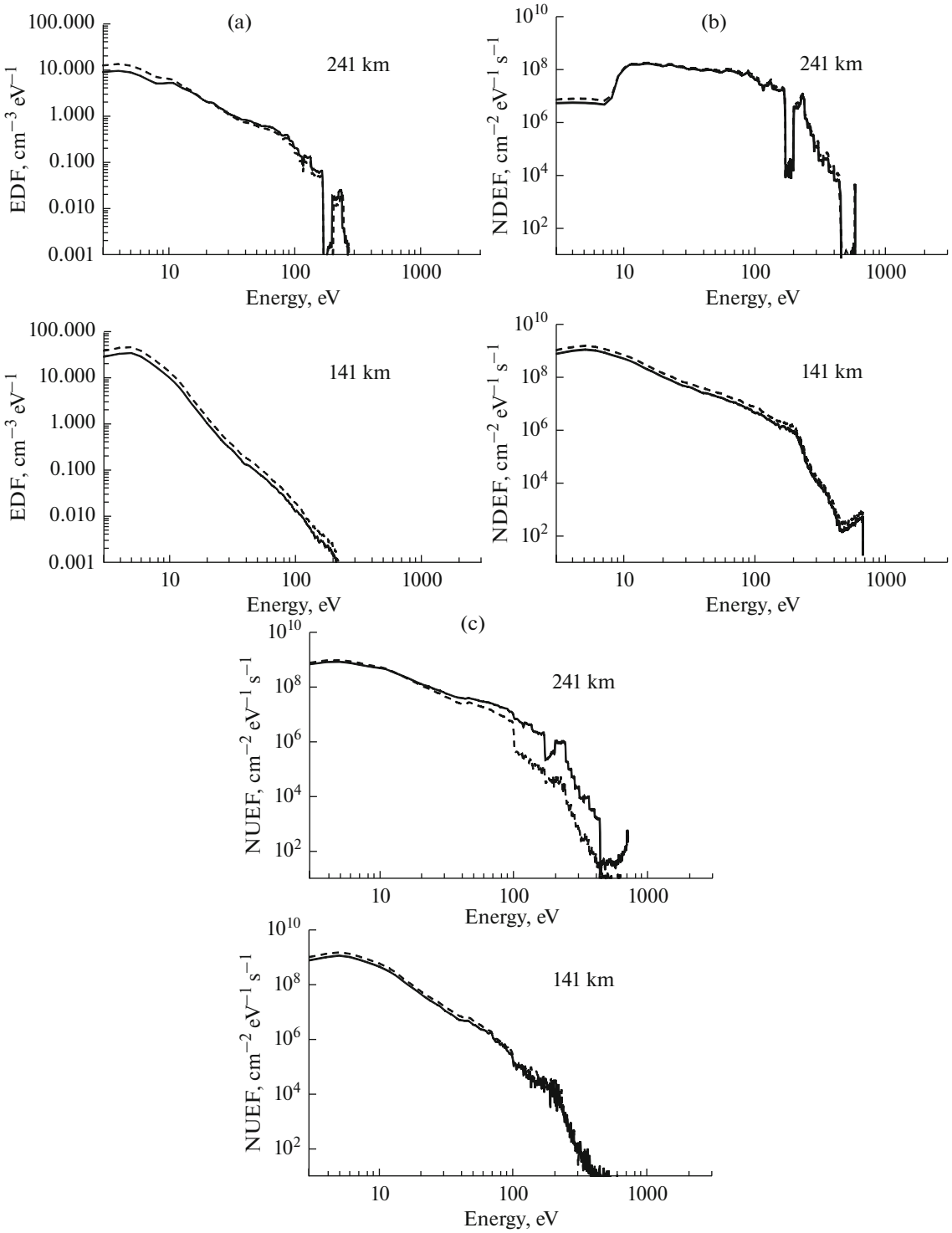

Fig. 2. (a) Electron kinetic energy distribution function (EDF) at an altitude of 241 km (top panel) and 141 km (bottom panel). Electron EDFs calculated with taking into account the magnetic field are shown by solid lines and without taking them into account, by dashed lines. These calculations were carried out using the electron flux measured on May 10, 2010, at 07:43 using the ASPERA-3 instrument on board *MEX* as the flux precipitating on the upper boundary of the flux. (b) Energy spectra of the numerical downward electron flux (NDEF) at an altitude of 241 km (top panel) and 141 km (bottom panel). Electron fluxes calculated with taking into account the magnetic field are shown by solid lines and without taking it into account, by dashed lines. (c) Energy spectra of the numerical upward electron flux (NUEF) at an altitude of 241 km (top panel) and 141 km (bottom panel). Electron fluxes calculated with taking into account the magnetic field are shown by solid lines and without taking it into account, by dashed lines.

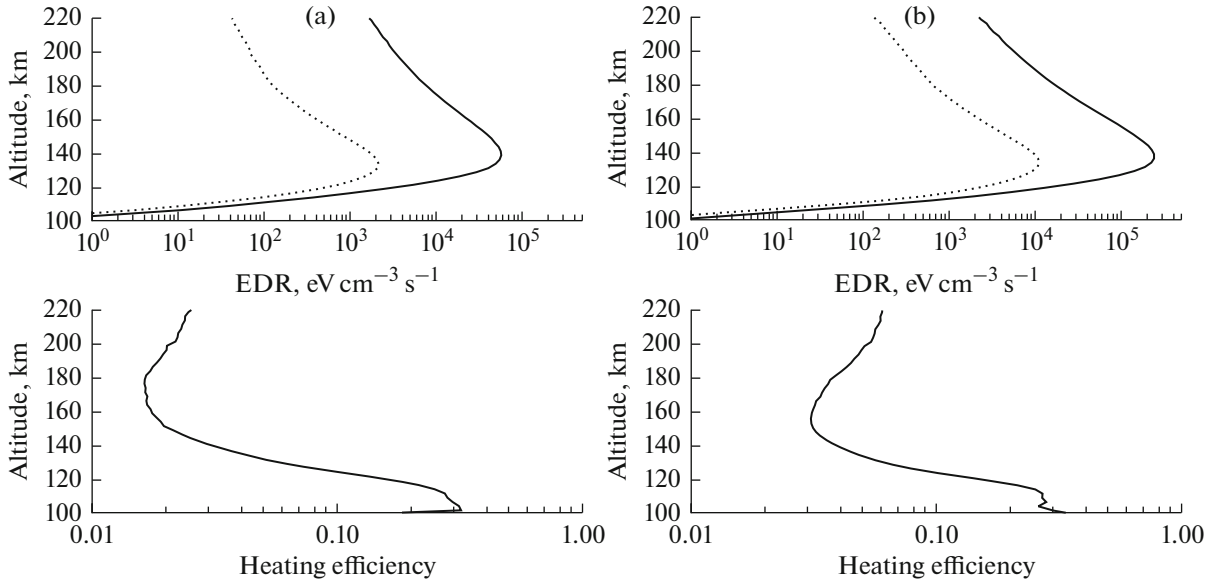

Fig. 3. (a) *Top panel:* the altitude profile of the electron energy deposition rate (EDR) due to collisions with atmospheric gas is shown by the solid line. Heating rate of the atmospheric gas by the precipitating electrons is shown by the dashed curve. *Bottom panel:* the altitude profile of the atmospheric gas heating efficiency (the ratio of deposition and heating rates presented in the top panel) by precipitating electrons. (b) The same as in Fig. 3a, but without taking into account the residual magnetic field.

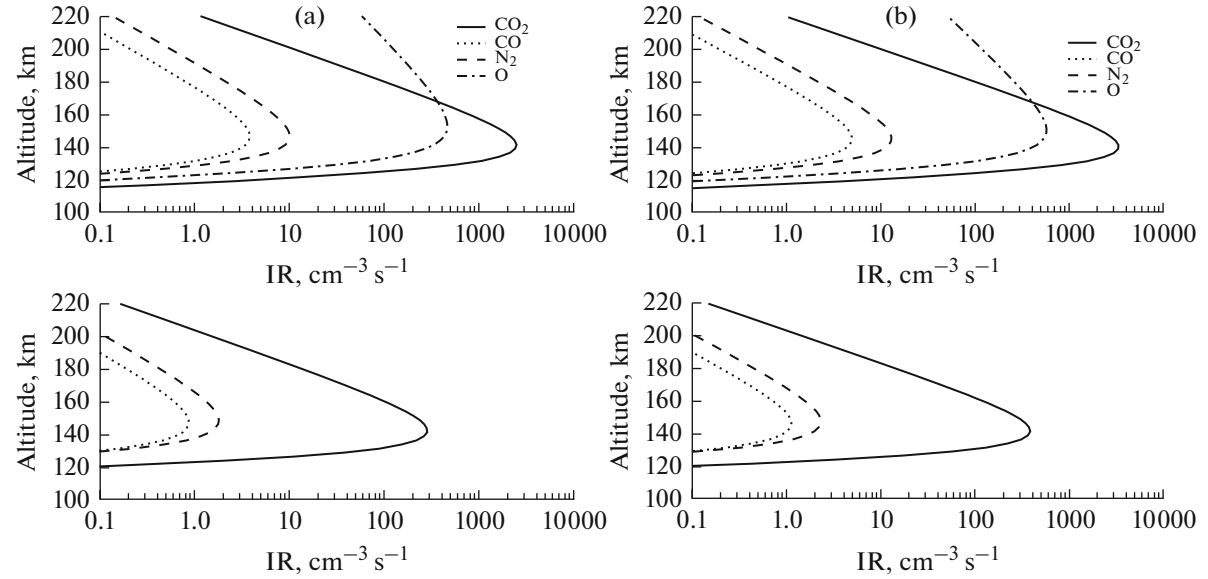

Fig. 4. (a) Altitude profiles of ionization of atmospheric components by the flux of precipitating electrons. *Top panel:* direct ionization rates (IR) of the main atmospheric components CO_2, CO, N_2, and O. *Bottom panel:* dissociative ionization rates (DIR) of atmospheric molecules. (b) The same as in Fig. 4a, but without taking into account the residual crustal magnetic field.

Figures 5–7 show the results of calculations of the penetration of monoenergetic electron fluxes with characteristic energies of 10 and 100 keV into the upper Martian atmosphere. In Fig. 5a, solid lines represent the electron kinetic energy distribution function (EDF), and Figs. 5b and 5c show the energy spectra for the downward and upward electron fluxes, respectively. From the analysis of the data presented in Fig. 5, it can be seen that in both cases as the flux penetrates deeper into the atmosphere its EDF changes significantly, i.e., a thermal core is generated and the distribution in the region of initial high energies decreases. The analysis of downward and upward electron fluxes demonstrates that for the case of a mon-

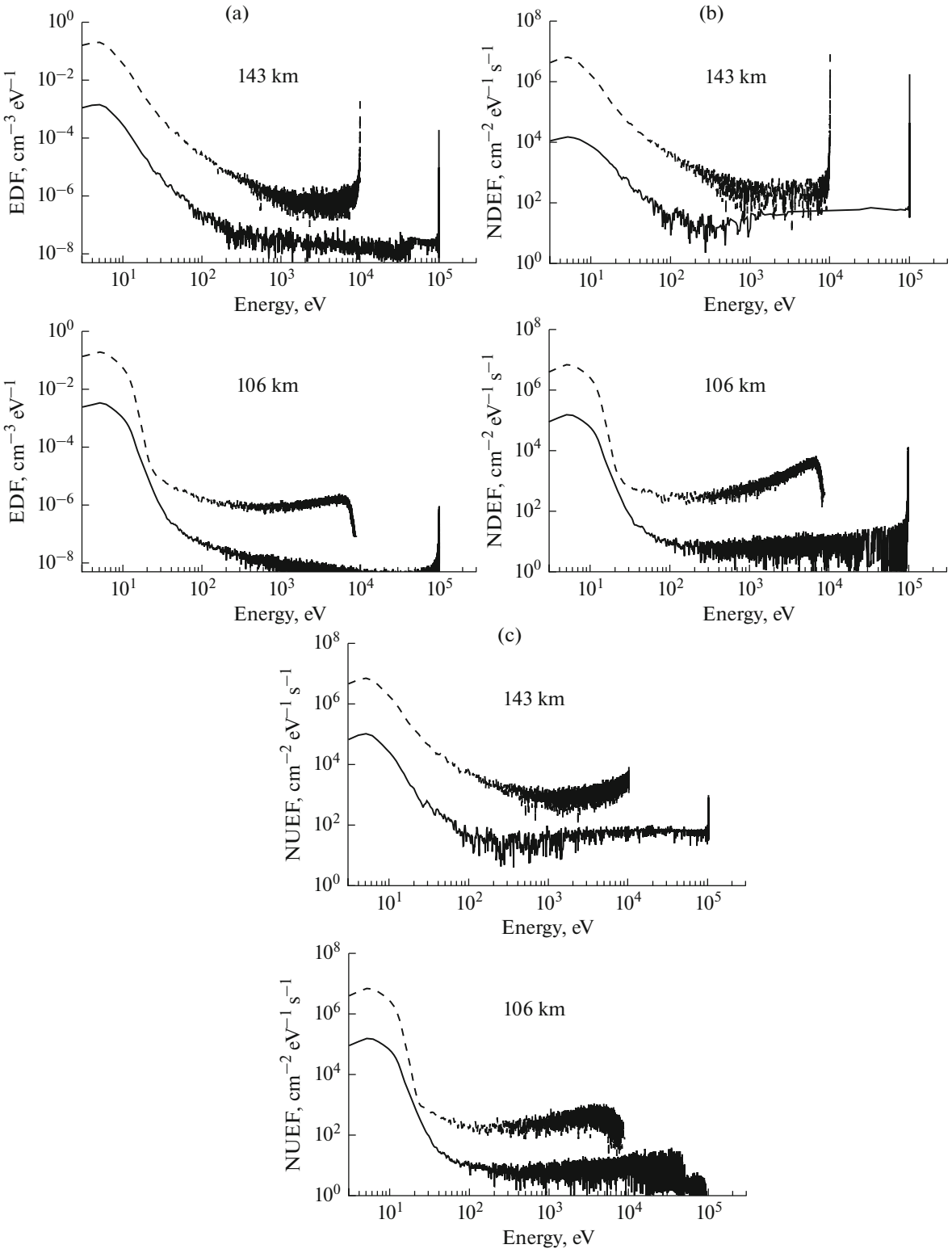

Fig. 5. (a) Electron kinetic energy distribution function (EDF) at an altitude of 143 km (top panel) and 106 km (bottom panel). For the case of precipitation at the upper boundary of the model of a monoenergetic flux with an energy of 100 keV, the calculated electron EDFs are shown by solid lines and for the case of a monoenergetic flux of 10 keV, by dotted lines. (b) Energy spectra of the numerical downward electron flux (NDEF) at an altitude of 143 km (top panel) and 106 km (bottom panel). (c) Energy spectra of the numerical upward electron flux (NUEF) at an altitude of 143 km (top panel) and 106 km (bottom panel).

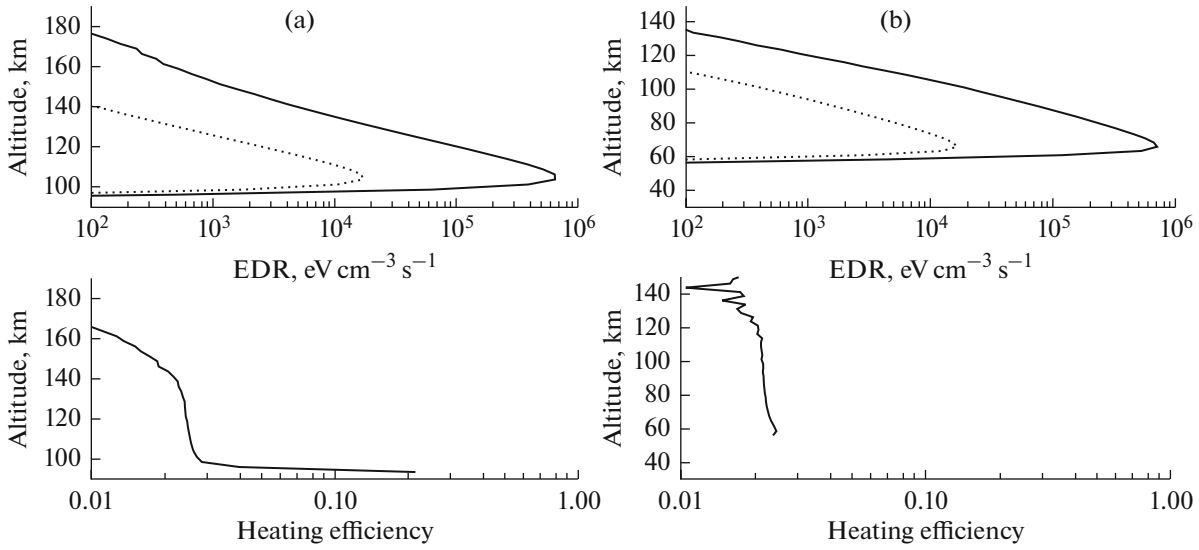

Fig. 6. (a) Top panel: the altitude profile of the energy deposition rate (EDR) due to collisions with atmospheric gas of the precipitating monoenergetic electron flux with $E_0 = 10$ keV is shown by the solid line. Heating rate of the atmospheric gas by the precipitating electrons is shown by the dashed curve. Bottom panel: the altitude profile of the atmospheric gas heating efficiency (the ratio of deposition and heating rates presented in the top panel) by the precipitating electrons. (b) The top panel: the altitude profile of the energy deposition rate (EDR) due to collisions with atmospheric gas of the precipitating monoenergetic electron flux with $E_0 = 100$ keV is shown by the solid line. Heating rate of the atmospheric gas by the precipitating electrons is shown by the dashed curve. Bottom panel: the altitude profile of the atmospheric gas heating efficiency (the ratio of deposition and heating rates presented in the top panel) by the precipitating electrons.

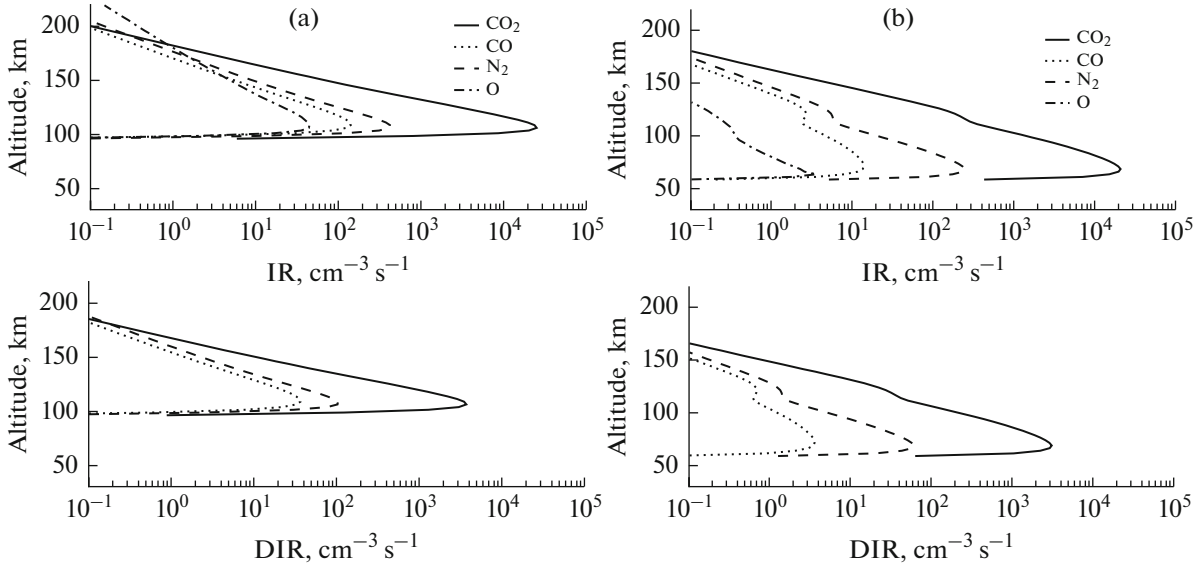

Fig. 7. (a) Altitude profiles of ionization of atmospheric components by the monoenergetic flux of precipitating electrons with $E_0 = 10$ keV. Top panel: direct ionization rates (IR) of the main atmospheric components (CO_2, CO, N_2, and O). Bottom panel: dissociative ionization rates (DIR) of atmospheric molecules. (b) Altitude profiles of ionization of atmospheric components by the monoenergetic flux of precipitating electrons with $E_0 = 100$ keV. Top panel: the direct ionization rate (IR) of the main atmospheric components (CO_2, CO, N_2, and O). Bottom panel: dissociative ionization rates of atmospheric molecules.

oenergetic flux with an energy of 10 keV the reflected energy flux reaches 24% and for a monoenergetic flux with an energy of 100 keV, 10%.

Solid lines in top panels of Figs. 6a and 6b show the altitude profile of the energy deposition rate due to elastic, inelastic, and ionization collisions with atmospheric gas of the precipitating monoenergetic electron flux with $E_0 = 10$ and 100 keV, respectively, and the altitude profile of the atmospheric gas heating rate by precipitating electrons is shown by dotted lines. The

bottom panels of Figs. 6a and 6b show the altitude profiles of the heating efficiency of the atmospheric gas (the ratio of the deposition and heating rates presented on the top panel) by the precipitating electrons with $E_0 = 10$ and 100 keV, respectively. It should be noted that the monoenergetic flux with $E_0 = 100$ keV penetrates much deeper into the Martian atmosphere and the electron energy deposition peak is recorded at an altitude of ~70 km, while the energy flux deposition peak with $E_0 = 10$ keV is detected at an altitude of ~105 km. It can be seen that the heating efficiency varies significantly with altitude, and the shape of the curves and their values differ significantly for the cases with $E_0 =$ 10 and 100 keV. For the low-energy case ($E_0 = 10$ keV), the heating efficiency can reach values of 0.2, while for the case of $E_0 = 100$ keV its values do not exceed 0.025, which indicates the role of direct and dissociative ionization increases in the case of the penetration of a flux with $E_0 = 100$ keV deep into the atmosphere.

Figures 7a and 7b show the altitude profiles of ionization of atmospheric components by the monoenergetic flux of precipitating electrons with $E_0 = 10$ and 100 keV, respectively. It can be seen that an increase in energy from 10 to 100 keV generates peaks of both direct and dissociative ionization at altitudes much deeper in the Martian atmosphere, while the values of the ionization rates at altitudes of the corresponding peaks vary insignificantly. This fact is one of the reasons for the decrease in the heating efficiency noted above with the increase of the energy of precipitating electrons.

Note that in the case of diffuse auroral events caused by high-energy auroral electron fluxes during the passage of the solar coronal mass ejection plasma cloud electrons penetrate deep into the atmosphere, up to the altitudes of the middle Martian atmosphere. Such events are accompanied by additional absorption of the electron energy at altitudes of the middle atmosphere that lead to excitation and ionization of the main component (CO_2). Accordingly, the chemistry of the middle atmosphere expands because of excited and ionized precipitation products, which leads to local changes in both the chemical composition of the main and trace components of the middle atmosphere and its temperature conditions.

CONCLUSIONS

Typical auroral events in the Martian atmosphere, such as discrete and diffuse aurorae detected by UV spectrometers onboard ESA *Mars Express* and NASA *MAVEN*, were considered. Auroral electron kinetic energy distribution functions and energy spectra of the upward and downward electron fluxes were obtained by electron transport calculations using the kinetic Monte Carlo model. These characteristics of auroral electron fluxes make it possible to calculate the observed manifestations of auroral events on Mars. In particular, intensities of discrete and diffuse aurorae in the UV and visible wavelength ranges (Soret et al., 2016; Bisikalo et al., 2017; Gérard et al., 2017).

For these conditions of auroral events, the analysis was carried out, and the contribution of the fluxes of precipitating electrons to the heating and ionization of the Martian atmosphere was estimated. Numerical calculations showed that in the case of discrete auroral events the effect of the residual crustal magnetic field leads to a significant increase in the upward fluxes of electrons, which causes a decrease in the rates of heating and ionization of the atmospheric gas in comparison with the calculations without taking into account the residual magnetic field.

Diffuse auroral events are caused by the electron precipitation with energies up to 200 keV (Schneider et al., 2015). Accordingly, such events are accompanied by the electron penetration deep into the Martian atmosphere and by an increase in the rates of excitation and ionization up to the middle atmosphere.

Thus, it is necessary to take into account all the above-mentioned impact factors of auroral electron precipitation processes both in photochemical models of the Martian atmosphere and in the interpretation of observations of the chemical composition and its variations using the ACS instrument on board *ExoMars*.

ACKNOWLEDGMENTS

This work was supported by the Russian Science Foundation, project no. 15-12-30038.

REFERENCES

Barabash, S., Lundin, R., Andersson, H., Brinkfeldt, K., Grigoriev, A., Gunell, H., Holmström, M., Yamauchi, M., Asamura, K., Bochsler, P., et al., The Analyzer of Space Plasmas and Energetic Atoms (ASPERA-3) for the Mars Express mission, *Space Sci. Rev.*, 2006, vol. 126, pp. 113–164.

Bertaux, J.-L., Leblanc, F., Witasse, O., Quemerais, E., Lilensten, J., Stern, S.A., Sandel, B., and Korablev, O., Discovery of an aurora on Mars, *Nature*, 2005, vol. 435, pp. 790–794.

Bisikalo, D.V. and Shematovich, V.I., Precipitation of electrons into the upper atmosphere of a hot-Jupiter exoplanet, *Astron. Rep.*, 2015, vol. 59, no. 9, pp. 836–842.

Bisikalo, D.V., Shematovich, V.I., Gérard, J.-C., and Hubert, B., Influence of the crustal magnetic field on the Mars aurora electron flux and UV brightness, *Icarus*, 2017, vol. 282, pp. 127–135.

Brain, D.A., Halekas, J.S., Peticolas, L.M., Lin, R.P., Luhmann, J.G., Mitchell, D.L., Delory, G.T., Bougher, S.W., Acuña, M.H., and Rème, H., On the origin of aurorae on Mars, *Geophys. Res. Lett.*, 2006, vol. 33, p. L01201.

Bougher, S.W., Pawlowski, D., Bell, J.M., Nelli, S., McDunn, T., Murphy, J.R., Chizek, M., and Ridley, A., Mars Global Ionosphere-Thermosphere Model (MGITM): solar cycle, seasonal, and diurnal variations

of the Mars upper atmosphere, *J. Geophys. Res.: Planets*, 2015, vol. 120, pp. 311–342.

Decker, D.T., Kozelov, B.V., Basu, B., Jasperse, J.R., and Ivanov, V.E., Collisional degradation of the proton /H atom fluxes in theatmosphere: a comparison of theoretical techniques, *J. Geophys. Res.: Planets*, 1996, vol. 101, pp. 26947–26960.

Gérard, J.C., Soret, L., Libert, L., Lundin, R., Stiepen, A., Radioti, A., and Bertaux, J.L., Concurrent observations of ultraviolet aurora and energetic electron precipitation with Mars Express, *J. Geophys. Res.: Planets*, 2015, vol. 120, pp. 6749–6765.

Gérard, J.-C., Soret, L., Shematovich, V.I., Bisikalo, D.V., and Bougher, S.W., The Mars diffuse aurora: a model of ultraviolet and visible emissions, *Icarus*, 2017, vol. 288, pp. 284–294.

Jakosky, B.M., Grebowsky, J.M., Luhmann, J.G., Connerney, J., Eparvier, F., Ergun, R., Halekas, J., Larson, D., Mahaffy, P., McFadden, J., Mitchell, D.F., et al., MAVEN observations of the response of Mars to an interplanetary coronal mass ejection, *Science*, 2015, vol. 350, no. 6261. doi . doi 10.1126/science.aad0210

Leblanc, F. Witasse, O., Lilensten, J., Frahm, R.A., Safaenili, Ali, Brain, D.A., Mouginot, J., Nilsson, H., Futaana, Y., Halekas, J., Holmström, M., Bertaux, J. L., Winningham, J.D., Kofman, W., and Lundin, R., Observations of aurorae by SPICAM ultraviolet spectrograph on board Mars Express: simultaneous ASPERA-3 and MARSIS measurements, *J. Geophys. Res.: Planets*, 2008, vol. 113, no. A08311.

Lillis, R.J. and Brain, D.A., Nightside electron precipitation at Mars: geographic variability and dependence on solar wind conditions, *J. Geophys. Res.*, 2013, vol. 118, pp. 3546–3556.

Lillis, R.J., Fillingim, M.O., Peticolas, L.M., Brain, D.A., Lin, R.P., and Bougher, S.W., Nightside ionosphere of Mars: modeling the effects of crustal magnetic fields and electron pitch angle distributions on electron impact ionization, *J. Geophys. Res.*, 2009, vol. 114, p. E11009.

Lillis, R.J., Fillingim, M.O., and Brain, D.A., Three-dimensional structure of the Martian nightside ionosphere: predicted rates of impact ionization from Mars Global Surveyor magnetometer and electron reflectometer measurements of precipitating electrons, *J. Geophys. Res.*, 2011, vol. 116, p. A12317.

Lundin, R., Winningham, D., Barabash, S., Frahm, R.A., Holmström, M., Sauvaud, J.-A., Fedorov, A., Asamura, K., Coates, A.J., Soobiah, Y., et al., Plasma acceleration above Martian magnetic anomalies, *Science*, 2006a, vol. 311, pp. 980–983.

Lundin, R., Winningham, D., Barabash, S., Frahm, R.A., Andersson, H., Holmström, M., Grigoriev, A., Yamauchi, M., Borg, H., Sharber, J.R., et al., Ionospheric plasma acceleration at Mars: ASPERA-3 results, *Icarus*, 2006b, vol. 182, pp. 308–319.

Millour, E., Forget, F., Spiga, A., Navarro, T., Madeleine, J.-B., Montabone, L., Lefevre, F., Chaufray, J.-Y., Lopez-Valverde, M.A., Gonzalez-Galindo, F., et al. The MCD/GCM Development Team, the Mars Climate Database, MCD version 5.1, *The Eighth Int. Conf. on Mars*, Houston, TX: Lunar Planet. Inst., 2014, no. 1791, p. 1184.

Shane, A.D., Shaosui, X., Liemohn, M.W., and Mitchell, D.W., Mars night side electrons over strong crustal fields, *J. Geophys. Res.: Planets*, 2016, vol. 121, pp. 3808–3823.

Schneider, N.M., Deighan, J.I., Jain, S.K., Stiepen, A., Stewart, A.I.F., Larson, D., Mitchell, D.L., Mazelle, C., Lee, C.O., Lillis, R.J., Evans, J.S., Brain, D., Stevens, M.H., McClintock, W.E., Chaffin, M.S., et al., Discovery of diffuse aurora on Mars, *Science*, 2015, vol. 350, no. 6261. doi 10.1126/science.aad0313

Shematovich, V.I., Bisikalo, D.V., Gérard, J.-C., Cox, C., Bougher, S.W., and Leblanc, F., Monte Carlo model of electron transport for the calculation of Mars day-glow emissions, *J. Geophys. Res.: Planets*, 2008, vol. 113, p. E02011.

Shirai, T., Tabata, T., and Tawara, H., Analytic cross-sections for electron collisions with CO, CO_2, and H_2O relevant to edge plasma impurities, *At. Data Nucl. Data Tables*, 2001, vol. 79, pp. 143–184.

Soret, L., Gérard, J.C., Libert, L., Shematovich, V.I., Bisikalo, D.V., Stiepen, A., and Bertaux, J.L., SPICAM observations and modeling of Mars aurora, *Icarus*, 2016, vol. 264, pp. 398–406.

Translated by O. Pismenov